A novel incomplete sparse least square optimized regression model for abdominal mass detection in ultrasound images

Shivshankar Sambhajirao Kore & Ankush B. Kadam

Evolutionary Intelligence

ISSN 1864-5909

Evol. Intel.
DOI 10.1007/s12065-020-00431-7

Springer

Evolutionary Intelligence
https://doi.org/10.1007/s12065-020-00431-7

SPECIAL ISSUE

A novel incomplete sparse least square optimized regression model for abdominal mass detection in ultrasound images

Shivshankar Sambhajirao Kore[1] · **Ankush B. Kadam**[2]

Received: 20 April 2018 / Revised: 15 February 2020 / Accepted: 21 May 2020

Abstract

One of the recent ways of checking the internal organs such as kidneys, gallbladder, liver, and spleen is using an abdominal US image. US image is more familiar for its unique characteristics like radiation-free, safe, cheaper and faster. However, the thing to be considered is that US images cannot grant a precise view of affected regions. More particularly the unprocessed US images comprise a lot of embedded noises. Thus the digital processing is a promising result for improving the quality of US images. This paper intends to propose a novel model for abdominal masses detection with US images. This detection model comprises two phases: feature extraction as well as Classification. In the feature extraction process, texture features are extracted from the US image by AGLOH. Then in the classification stage, the optimized ISLSR model is used to detect whether the mass is present in the abdomen or not, where the coefficient matrix is optimally tuned using a new hybrid Lion and Whale Optimization algorithm. The performance analysis of the proposed method is compared with existing techniques such as GLCM-SVM, GLCM-NN, GLCM-LDCA, AGLOH-SVM, AGLOH-NN, AGLOH-LDCA, AGLOH-ISLSR-LA, and AGLOH-ISLSR-WOA. The performance of the developed method is analyzed in terms of both positive as well as negative measures: the positive measures include accuracy, sensitivity, specificity, and precision, NPV, F_1 Score, and MCC. The negative measures include FPR, FNR, and FDR, and the efficiency of the proposed model is proved.

Keywords Abdominal mass diagnosis · US image · AGLOH · ISLSR model · Performance measures

Abbreviations

ARPKD	Autosomal recessive polycystic kidney disease
MRI	Magnetic resonance imaging
CT	Computed tomography
RUSBOOST	Random under-sampling boosting
FROC	Free response operating characteristics
HMBS	Homogeneity modified Bayes shrink
DPM	Deformable part models
CAP	Computer-aided prediction
FPR	False positive rate
FNR	False negative rate
FDR	False discovery rate
NN	Neural network
OBNLM	Optimize Bayesian non-local mean filter
NPV	Negative predictive value
MCC	Mathews correlation coefficient
AGLOH	Adaptive gradient location and orientation histogram
GLCM	Grey level co-occurrence matrix
LDCA	Link discovery based on correlation analysis
SVM	Support vector machine
SD	Standard deviation
BANN	Back propagation artificial neural network
US	Ultrasound
ISLSR	Incomplete sparse least square regression
ALN	Axillary lymph node
CAD	Computer-aided diagnosis
MS-GGVF	Multi-scale generalized gradient vector flow

✉ Shivshankar Sambhajirao Kore
koreshiv@gmail.com

[1] Department of Physics, A. P. Shah Institute of Technology, Thane, India

[2] Department of Physical Sciences, Jawahar Arts, Science and Commerce College, Andoor, India

Published online: 12 June 2020

1 Introduction

Basically, the abdominal mass meant either gradual extension or swelling, especially in human anatomy. Based on the location, the abdominal mass might get varied, it may be caused by many reasons like hepatomegaly, splenomegaly, pancreatic [1] mass, retroperitoneum, etc. [2]. Abdominal masses are normally unpredictably viewed on from the physical consideration of daily routine. It would also detect as abdominal imaging [3, 4]. The abdominal masses are basically more extensible, which ranges from 'benign' to 'neoplastic' that are often originates from the cavity of intra-abdominal [5]. The related prenatally as well as renal mass is actually unilateral, which obtains from either 'obstruction' junction or 'vesicoureteral reflux.' Moreover, 'hydronephrosis' often occurs due to 'multicystic' dysplastic kidneys, and it is determined as numerous non-communicating cysts. The size of the cyst normally differs (minimum to normal renal tissue). The mass that termed as 'Bilateral renal masses' is found on an investigation or from imaging, which is concerned with a specific disease named 'ARPKD.' The appearance of this disease varies from hyperplasia degree of the assembling tubules that further might be perceived in utero or it would be advanced from the individual's childhood.

The initial examination or investigation of suspected abdominal mass is indicated with the aid of imaging studies named 'Plain abdominal Radiographs'. This study of radiographs must aid in describing the location of the mass and its corresponding density, which also might grants either valued information or data in correspondence with an intestinal obstruction that also comprises the presence of lack of air or multi-air fluid levels in the rectum. With this, the classification [6–12] plays a major role in the specification of tumor occurrence like 'teratomas', 'neuroblastoma', and 'lithiasis'. Imaging is a leading technique for sampling non-palpable organ abnormalities, along with the determination of extended cancer tumors [13, 14], which are local as well as loco-regionally. The therapy responses establish a subordinate role in imaging. Numerous imaging modalities are in progress that includes: 'MRI' [15, 16] that shows promising results for noticingoccult cancers, which is also more useful in determining the extension of malignant disease. Likewise, CT [17] scan is more helpful in viewing the lung tumors than repeated chest x-rays. The imaging technique effectively shows the size, shape, and location of tumors that present in the lung and also aids in identifying the prolonged lymph [18] nodes that comprise cancer that has feast from the lung.

Further, the imaging named US imaging is subsequently aided as an important supplement to physical analysis [19, 20] for the evaluation of varied masses. The US can distinguish the cystic that present in solid masses and with this, it aids in discriminating the benign from the solid masses like malignant solid masses. Moreover, it can detect certain non-palpable carcinomas, which are missed out by other imaging models, and this is more efficient for screening breast cancer [21–23], which is already proven from many researchers. It achieves due to its specific real-time ability, and further the US images [24, 25] also becomes the important model of guiding the procedure of percutaneous interventions on cancer diseases. Generally, the count of cancer detection models that uses US imaging [26–30] is available more, which is categorized on the basis of un-structural morphology, sequence analysis, biochemical characteristics, etc. Even though the proficiency of US imaging is already proved in enormous cancer diagnosing models; only little contributions have been adopted in diagnosing abdominal masses, which is mentioned in the literature section. Thus this has a large scope for future researches in diagnosing modality of abdominal masses with the aid of US images. This paper propose novel Incomplete Sparse Least Square Regression (ISLSR) optimization for abdominal masses detection with US images which has been used in the various field such as [31–34].

This paper proposes a novel model for abdominal masses detection with US images. This detection model comprises two phases: feature extraction as well as Classification. In the feature extraction process, texture features are extracted from the US image by AGLOH. Then in the classification stage, the optimized ISLSR model is used to detect whether the mass is present in the abdomen or not, where the coefficient matrix is optimally tuned using a new hybrid Lion and Whale Optimization algorithm. The performance analysis of the proposed AGLOH method is compared with existing techniques such as GLCM-SVM, GLCM-NN, GLCM-LDCA, AGLOH-SVM, AGLOH-NN, AGLOH-LDCA, AGLOH-ISLSR-LA, and AGLOH-ISLSR-WOA. The rest of the paper is organized as follows: Sect. 2 reviews the literature work, Sect. 3 explains the stages of abdominal mass detection, Sect. 4 discusses the overall proposed model, Sect. 5 discusses the results obtained, and Sect. 6 concludes the paper.

2 Literature review

2.1 Related works

In 2017, Kozegar et al. [21] have developed a detection model, that too in multi-stage for the cancer detection scenario in images like 'ABUS' images. Very first speckle noises were reduced, and it was attained with the application of a de-speckling method called "OBNLM." Next,

to this, a novel protocol was portrayed for the purpose of detecting the initial candidates as the masses boundary, and it was on the basis. Some features like 'roundness', 'hypoechogenicity', 'area strength' and 'contour strength' were used for the reduction of falsely produced isocontour of isocontours. Further, the subordinate candidates were then progressed with the aid of a cascade classifier, and some of the base classifiers were 'RUSBoost', that was developed for working on imbalanced datasets. The developed model has investigated on the basis of 'FROC' and the results have proved its better performance over other models.

In 2016, Elyasi et al. [22] have developed an algorithm for reducing the speckle noise present in breast cancer images (US). A combination of 'homogeneity filtering' and model termed 'modified Bayes shrink model' was employed for the elimination of noise. Firstly, the intensity of pixels was replaced with others and then the threshold value was employed for the modification of the Bayes shrink model. This was worked out for the discrimination of homogeneous regions that contains speckle noise, which was attained from the filtering process. The developed 'HMBS' method has proved its efficiency over conventional models.

In 2016, Gu et al. [26] have developed an automated algorithm, which could segment the 3D ultrasound volumes. The segmentation process took place in three types including 'mass/cist' tissue, 'fibro-glandular tissue' and 'fatty tissue' respectively. The evaluation was done to analyze the efficiency as well as the consistency of the developed model. This was achieved by employing them over a database with 21 test cases of breast US images. The outcome of the investigation has shown the excellence of the proposed model by distinguishing the responsible tissues and moreover it has achieved in the classification of tissues as well. Overall, the model has attained excellent consistency and potential in distinguishing the tissues.

In 2014, Pons et al. [27] have developed an object detection model and a model named 'DPM. This was for detecting whether the image presents any lesions. a data set of 326 images were utilized by many patients. The developed model has shown its efficiency over conventional models by detecting the lesion precisely. The obtained sensitivity of the model is high with 86%, 'False positive detection' of 0.28 (per image). Further, the proposed model has reviewed its efficiency in correspondence with 'malignant lesion detection.'

In 2017, Moon et al. [28] has proposed a model termed CAP model that has used the nearby tissue features in 'US' images. The method has determined for defining the ALNstatus in cancer like breast cancer. The dataset that used presents 114 cases (breast cancer) and 49 of 114 were 'ALN metastasis'. Finally, the prediction model has trained as well as tested. From the outcome, the textural feature extracted from the nearby tissue has reviewed excellent performance than the other feature sets such as morphology and intensity.

In 2017, Abdel-Nasser et al. [6] have developed the usage of a model namely 'super-resolution approach' that has also exploited the complementary data granted by multi-images from the identical target. The proposed CAD model has contained four phases such as 'super-resolution computation', 'Extraction of the region of interest,' 'feature extraction' and 'classification'. They have assessed the performance of texture models (five) with the proposed CAD model. They have also reviewed the performance of the developed model has outperformed the existing classification model.

In 2014, Le [13] had developed a new deformable snake model termed as MS-GGVF for segmentation purposes. The important role of this developed model the rectification of the challenges such as 'spurious boundary attenuation' as well as setting SD of filter named Gaussian filter. For the assessment of the external force vector field, they have developed a vector flow formulation algorithm. The investigation results have proved the efficiency of the developed model.

In 2016, Singh [7] have developed a novel classification model with a combination of two: unsupervised learning modality as well as a supervised learning model. 'Fuzzy c-mean clustering' is utilized as the unsupervised learning technique and BANN is utilized as the unsupervised learning model. The proposed model was for the classification of tumors such as benign as well as malignant tumors in US images (breast). The investigation was performed by analyzing the count of US images. The results of the model proved its efficiency over other conventional methods.

2.2 Motivation

Table 1 reviews the features and challenges of numerous lesion detection model in US images. CADe model [21] could be utilized in real-world applications and also had the ability to obtain satisfactory results. However, closed iso-contour identification from all the nearby boundaries was impossible. HMBS model [22] achieves wild running time and further improves the quality of the image, but the image registration process was a tedious task. DPM model [27] notices the accurate lesion, but the correct evaluation of the bounding box was not possible. CAP model [28] improves the texture feature set and grants useful information for predicting the status of ALN. Nevertheless, the forecasting of the unknown region (thickness) was difficult. CAD model [6] improves the performance of texture image and 'Area Under the receiver operates characteristic Curve (AUC)' values, but the assessment of related models was impossible. Gradient Vector flow Computation algorithm [13] was efficient for the ablation of diseased tissues, but it needs more

Table 1 Features and challenges of various lesion detection model in US images

References	Method	Features	Challenges
Kozegar et al. [21]	CADe model	Achieves high sensitivity It can grant satisfactory results	Cancerous masses may miss while analyzing Could not find the closed iso-contour from nearby boundaries
Elyasi et al. [22]	HMBS model	Attains fast running time Enhances the performance by improving the quality of the image	Enhanced smoothing leads to image blurring Image registration process is a complex process
Gu et al. [26]	Morphological reconstruction with Sobel operator and watershed transform	Distinguish fatty and non-fatty tissues Outperforms in the combined imaging model	Difficult in the process of Shadow separation from the lesion Requires additional manual corrections for automatic segmentation
Pons et al. [27]	DPM model	Can implement in clinical applications Correctly detects the lesions	Cancer detection is impossible by this model Cannot recognize satisfactory results impossible to assess the boundary box accurately
Moon et al. [28]	CAP model	It provides useful data for the ALN prediction status Enhances the performance of the texture feature set	Prediction of unknown regions (thickness) in the image is impossible Seeing additional features may often provide poor performance
Abdel-Nasser et al. [6]	CAD model	Enhances the AUC value Improves the performance of the texture model	Cannot evaluate other medical image modalities CAD tool tunes with more sensitivity lead to poor performance
Le [13]	Gradient Vector flow Computation algorithm	Useful for other image models It can utilize for the ablation of diseased tissues	Low accuracy rate High computational time
Singh [7]	Neural Network Classifier	Learning capability is more, and reprogramming is not necessary Simply implemented and is parallel in nature	It needs additional training for operation purposes It requires to be emulated The processing of a large NN model requires more time

computational time. Neural Network Classifier [7] can implement easily, and it was naturally parallel. However, it necessitates additional training for the achievement of better results. Hence, to overwhelm all such drawbacks, it was essential for an effective abdominal mass detection model. Figure 1 demonstrates the taxonomy classification of lession detection model.

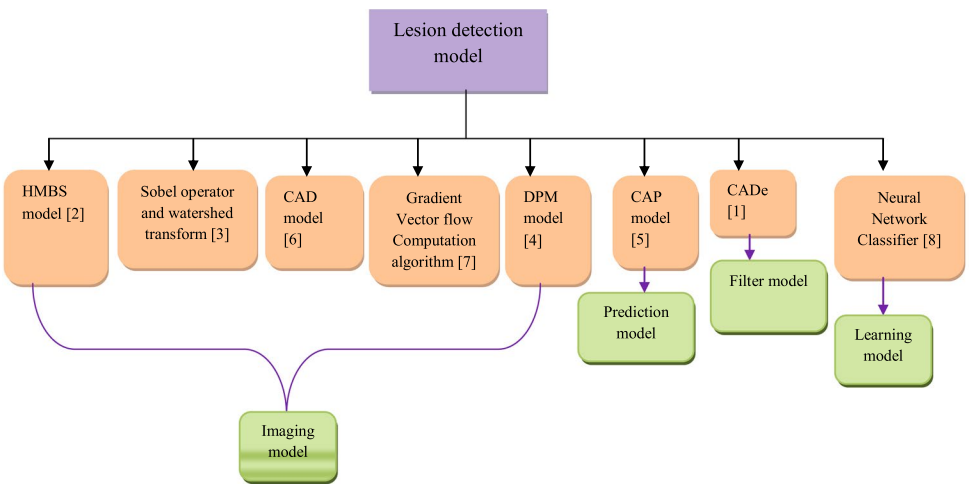

Fig. 1 Taxonomy classification of lession detection model

3 Stages of abdominal mass detection

3.1 Feature extraction stage

Consider the input US image as $I_I(u, v)$, from which the features are extracted using the AGLOH mechanism. AGLOH extracts the characteristics on the basis of orientation and texture invariants, whereas the conventional GLOH descriptor [35] estimates several discrete orientations to combine it into orientation invariant. The texture invariant characteristics are established with an adaptive filter, which is processed in the early stage of the GLOH method.

Hence, this paper intends to proceed with adaptive bilinear filtering. The filtering is meant for texture smoothing of $I_I(u, v)$. The $f\left(I_I(u, v)\right)$ parameter is defined in Eq. (1). The resultant filter image is denoted as Z_n^F, from which GLOH descriptor extracts the features.

$$f\left(I_I(u, v)\right) = z_{11}uv + z_{10}u + z_{01}v + z_{00} \tag{1}$$

In GLOH descriptor, the grid comprises a circular ring P, which centers the feature points. The rings involved in q regions are consistently contributed along with Q directions. A region R_{xy} is considered, where $R_{x,y} \in Z_n^F$; $x = 1, 2, \ldots, P$ and $y = 0, 1, \ldots, Q-1$. Further, the circular inner region is divided into Q radial segments by defining more or single regions as $R_{0,y}$ and $R_{0,0}$ respectively. For v descriptor vector, a function $\Psi(v)$ is mentioned as $\Psi(v) = 0$, if and only if $R_{0,0}$ is defined and 1 if $R_{0,y}$ is defined.

The histogram orientation for all regions by gradient magnitude is evaluated in quantized direction Q and b_r, the bin value for all-region, where $r = 0, 1, \ldots, Q-1$ is evaluated via Gaussian kernel density evaluation, which is the attained enhanced evaluation.

$$b_{x,y}^r = \frac{1}{\sqrt{2\pi\sigma}} \sum_{p \in R_{x,y}} g_{mg}(p) e^{-\frac{\left(M_2 \prod (G_{or}(p) - Q_r)\right)^2}{2\sigma^2}} \tag{2}$$

where $g_{or}(p) g_{mg}(p)$, denotes the orientation as well as gradient magnitude of p pixel in $R_{x,y}$ region with $x = 0, 1, \ldots, P$ and $y = 0, 1, \ldots, Q-1$, respectively, $Q_r = \frac{2\pi}{Q} r$ refers to the bin center r th and $c \in R^+$ denotes the standard deviation with $\sigma = \frac{2\pi}{Q} c$. The parameter $M_l(z)$ defines the l periodicity of length, which is determined in Eq. (3). Equation (4) specifies the block histogram, where, $\oplus$ refers to the concatenation operator, in such a way that the final descriptor vector v is gained by concatenating the histograms.

$$M_l(z) = \begin{Bmatrix} z & if \;\; z < \frac{l}{2} \\ l - z & otherwise \end{Bmatrix} \tag{3}$$

$$v_{x,y} = \bigoplus_{r=0}^{Q-1} b_{x,y}^{[y+r]Q} \tag{4}$$

The length of descriptor is given in Eq. (5). The circulation of the descriptor is achieved by a δk factor as mentioned in Eq. (6), where $\delta k = \frac{2\pi}{Q}$ and $v_{0,k}$ is $v_{0,k} = \bigoplus_{r=0}^{Q-1} b_{0,y}^{[r+k+y]Q}$.

$$l = P(PQ + 1 + (Q-1)\Psi(v)) \tag{5}$$

$$v_{\delta k} = \begin{Bmatrix} \bigoplus_{r=0}^{P} \bigoplus_{s=0}^{Q-1} v_{r,[k+s]Q} & if \;\; \Psi(v) = 1 \\ v_{0,k} \bigoplus_{r=1}^{P} \bigoplus_{s=0}^{Q-1} V_{r,[k+s]Q} & otherwise \end{Bmatrix} \tag{6}$$

The distance between v and $\bar{v}$ features are specified in Eq. (7), where, $D_T(v, \bar{v})$ refers to the estimation of usual distance. Hence the extracted features from the abdominal image are denoted as $F^{GLOH} = X = \left[X_1, X_2 \ldots X_K\right] \in \Re^{m \times n}$ where K specifies the entire number of features.

$$\hat{D}_T\left(v, \bar{v}\right) = \min_{k=0,1,\ldots,Q-1} D_T\left(v, \overline{v_{\delta k}}\right) \tag{7}$$

3.2 Classification stage

The extracted features F^{GLOH} are given for classification purposes to detect the mass presentation. For this, ISLSR [36] classification model is imposed in this paper. The features are specified in a matrix format, and every column in F^{GLOH} is specified as the feature vector, which consists of features of the abdominal US image, and the entities of $A_i = \left[m_{1i}, \ldots \ldots m_{di}\right]^U$, which takes either 0 or 1, which is shown in Eq. (8).

$$m_{ji} = \begin{cases} 1, \; if \; h_i \; belongs \; to \; jth \; class \\ 0, \; otherwise \end{cases} \tag{8}$$

If $F_o^{GLOH} \in \Re^{n \times N}$ is considered as another data matrix with unknown class labels, these ISLSR model asses the ISLSR model parameters and the unknown abdominal label matrix that is denoted by $L_o \in \Re^{d \times N}$ in correspondence, where n and d denotes the number of features and number of abdominal mass detection with F_o^{GLOH} matrix, which is on the basis of F^{GLOH}, F_o^{GLOH} and L data matrices. The optimization problem is evaluated as per Eq. (9), where B denotes the regression coefficient matrix that will be optimally tuned.

To make feature selection of abdominals in a well-realized form, there is an effective corresponding way to do some columns B to zero. At last, the mentioned Eq. (9) is reformulated by striking a norm penalty $m_{2,1}$ in terms of B onto the objective function. This functions shrinking of entries, i.e., the entries of B column shrink to zero, where determines the summation of m_2 norms of B. Hence the

features related to non-zero columns of B are utilized for abdominal mass detection. The reformulated ISLSR model is defined in Eq. (10), where $L_o > 0$ refers to all entries of L_o are non-negative, 1 denotes the vectors with entire entries and λ denotes a parameter named 'trade-off' parameters.

$$\arg\min_{B,L_o} ||\left[L\ L_o\right] - B\left[F^{GLOH}\ F_o^{GLOH}\right]||_H^2 \tag{9}$$

$$\arg\min_{L_o,B} ||\left\{L\ L_o\right\} - B\left\{F^{GLOH}\ F_o^{GLOH}\right\}||_H^2 + \lambda||B||_{2,1} \quad so\ that.\ L_o^U 1 = 1, L_o \geq 0 \tag{10}$$

Here the variable B is optimized to distinguish the image using Hybrid Lion Algorithm and Whale Optimization Algorithm during classification. The classification results in whether the image is normal or abnormal.

4 Overall abdominal mass detection model

4.1 Proposed mass detection system

The proposed mass detection system is illustrated in Fig. 2. The input US image is given for the detection of mass that present in the image. Basically, the proposed model works in two phases: Feature Extraction and Classification. Here, the features are extracted using the AGLOH method and classification is performed using a model named ISLSR model. In the feature extraction phase, some steps are followed. At

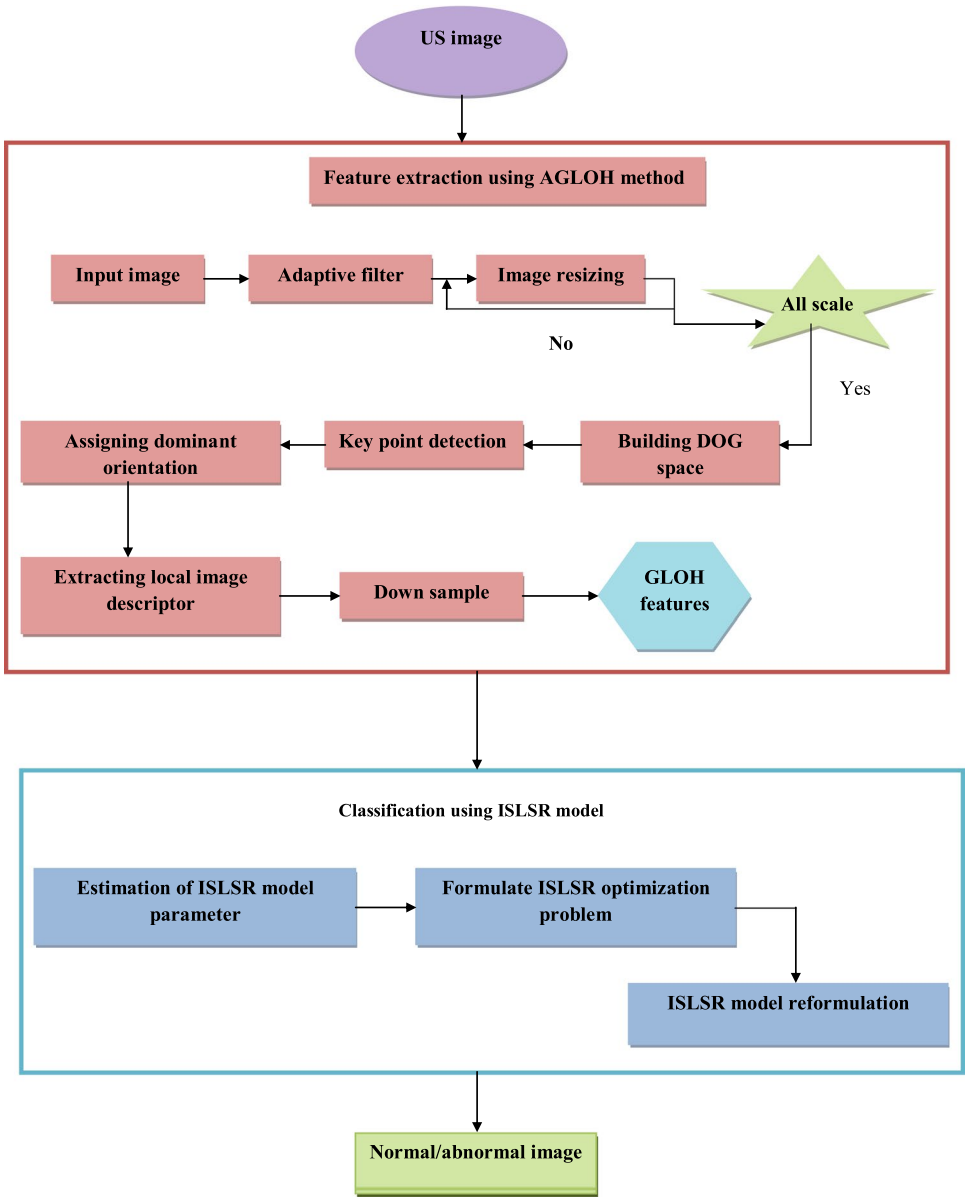

Fig. 2 Architecture of abdominal mass detection system

first, the given input image gets filtered, which is termed as an adaptive filtering process. Then the image is resized, and it builds the DOG space. The key points are detected in the next level and assign the dominant orientation. The local image descriptors are extracted from the image and results with the GLOH features.

The next phase is the classification. The extracted features from the feature extraction phase are given as input to the classification process. Here, three major steps must be followed as mentioned in the previous section. Initially, the model evaluates the ISLSR model parameter. Then the ISLSR optimization problem is formulated as per Eq. (9). Then the final step is the reformulation of the ISLSR model, which is given in Eq. (10). The classification results in the classified output, it tells whether the image is a normal image or abnormal image (with mass).

4.2 Proposed hybrid lion and whale optimization algorithm

Lion Algorithm [37] was developed on the motivation attained from unique social behavior (Territorial defense and territorial takeover) of the lion's.

In Lion Algorithm, the initialization process is indicated as pride generation and here the X^{male}, X^{female}, X^{nomad} are initialized. The variables x_l^{male}, x_l^{female} and x_l^{nomad} are the random vector elements of X^{male}, X^{female} and X^{nomad}, correspondingly lying within the maximum and the minimum values when $n > 1$ and $l = 1, 2, 3, \ldots L$. Moreover, L and its equivalent formula is demonstrated in Eq. (14). The decisions on the length of the lions are done using the integers m and n.

$$L = \begin{cases} n \quad n > 1 \ (general\ case) \\ m \ otherwise \ (Special\ case) \end{cases} \tag{11}$$

4.2.1 Fertility evaluation

It aids the hunting agents to avoid from being trapped into local optima. In this, a male lion X^{male} tends to become laggard with a raise in the L_r by one. The f^{ref} is attained while $f(X^{male}) > f^{ref}$. Moreover, while $L_r > L_r^{\max}$, territorial defense occurs and the values of X^{female} as $X^{female+}$ happens when S_r is higher than tolerance $S_r^{\max}$ (i.e. $S_r > S_r^{\max}$). As per Eqs. (12) and (13), the updating of $X^{female+}$ occurs, until the female generation count g_c achieve $g_c^{\max}$. In case of no $X^{female+}$ to replace X^{female}, subsequently X^{female} it is still fertile to generate cubs. The variable $x_k^{female+}$ and $x_l^{female+}$ shows k^{th} and l^{th} vector elements associated with the $r^{female+}$. The arbitrary integer k is created within the interval [1, L]. Moreover, the variable r_1 and r_2 that are devised within [0, 1].

$$s_l^{female+} = \begin{cases} s_k^{female+} & if\ l = k \\ s_l^{female} & otherwise \end{cases} \tag{12}$$

$$s_k^{female+} = \min\left[s_k^{\max}, \max\left(s_k^{\min}, \nabla_k\right)\right] \tag{13}$$

$$\nabla_k = \left[s_k^{female} + \left(0.1\, rd_2 - 0.05\right)\left(s_k^{male} - rd_1 s_k^{female}\right)\right] \tag{14}$$

4.2.2 Mating

In this, crossover and mutation is the fundamental step and secondary which comprise the gender clustering. Moreover, S^{male} and S^{female} experiences crossover and mutation to generate cubs. The nomad coalition generation and survival fight are sequenced by the territorial defense. In proposed algorithm, the mutation process of LA is updated using the spiral updating operation of the WOA algorithm [38] using Eq. (15), correspondingly.

$$\vec{X}(t+1) = \vec{F}' e^{pl}.\mathrm{Cos}(2\pi l) + \vec{X} * (t) \tag{15}$$

4.2.3 Lion operators

The chosen of the $S^{e-nomad}$ occurs by fulfilling the criteria shown in Eqs. (15)–(17).

$$f\left(X^{e-nomad}\right) < f\left(X^{male}\right) \tag{16}$$

$$f\left(X^{e-nomad}\right) < f\left(X^{m-cub}\right) \tag{17}$$

$$f\left(X^{e-nomad}\right) < f\left(X^{f-cub}\right) \tag{18}$$

4.2.4 Termination

The process execution gets terminated while any one of the following criteria expressed in Eqs. (18) or (19) is met. The count of generations N_f, maximum number of generations $N_f^{\max}$ and target error and e^T are utilized. The pseudo-code of the proposed algorithm is shown in Algorithm 1 and the flow chart of Hybrid LA-WOA is demonstrated in Fig. 3.

$$N_f > N_f^{\max} \tag{19}$$

$$\left|f\left(X^{male}\right) - f\left(X^{optimal}\right)\right| \le e^T \tag{20}$$

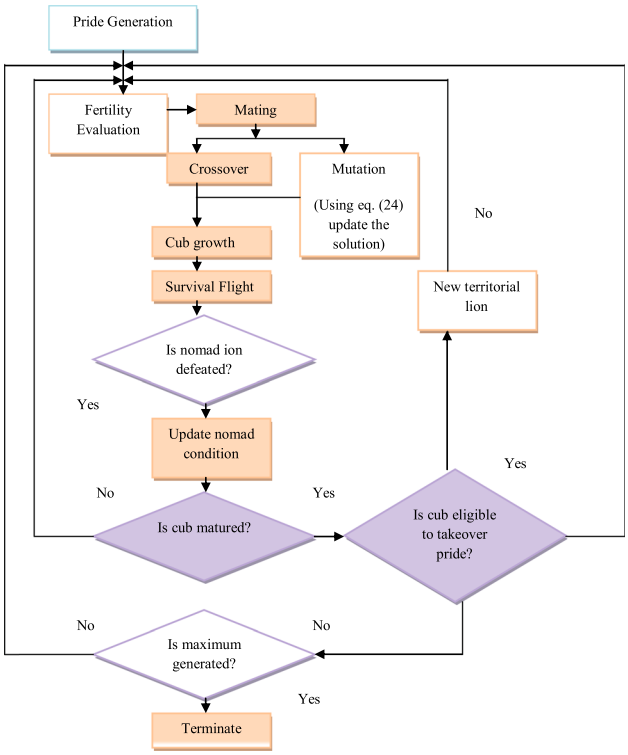

Fig. 3 Architecture of abdominal mass detection system

Steps	Algorithm 1: Pseudo-code of Proposed LA-WOA
Step 1:	Initialize X^{male}, X^{female} and X_l^{nomad}
Step 2:	Calculate $f(X^{male})$ $f(X^{female})$ and $f(X_l^{nomad})$
Step 3:	Allocate $f^{ref} = f(X^{male})$ and $t = 0$
Step 4:	Gather X^{female} and $f(X^{male})$
Step 5:	Fertility calculation is achieved
Step 6:	Carry out mating and reach the cub pool
	The mutation process of LA is updated using the spiral updating operation of the WOA algorithm using Eq. (15),
Step 7:	Accomplish X^{m-cub} and X^{f-cub} performing gender clustering
Step 8:	Allocate age of cub Ag^{cub} as 0
Step 9:	The cub growth function is simulated
Step 10:	Territorial defense is carried out and if the ensuing defense is 0, go to step 4
Step 11:	If $Ag^{cub} < Ag^{\max}$, go after step 9.
Step 12:	Perform territorial takeover and attain updated X^{male} and X^{female}
Step 13:	Raise N_f by one
Step 14:	In case of not meeting the termination criterion, go to step 4, or else terminate the process

5 Results and discussion

5.1 Simulation procedure

The proposed abdominal mass detection model was developed in MATLAB, and the results were discussed. The database with 20 images was used for the experimentation, which includes 12 normal images and 10 abnormal images. The proposed AGLOH feature extraction was compared with other models like AGLOH-SVM, AGLOH-NN, AGLOH-LDCA, AGLOH-ISLSR-LA, and AGLOH-ISLSR-WOA methods, whereas the proposed classification method was compared with other classification methods like LDCA [39], SVM [40] and NN [41], respectively. The performance of the developed method was analyzed in terms of both positive as well as negative measures. The positive measures include accuracy, sensitivity, specificity, and precision, NPV, F_1 Score, and MCC. The negative measures include FPR, FNR, and FDR. The outcome of the investigation has shown the efficiency of the proposed AGLOH-ISLSR method.

5.2 Feature performance

The effectiveness of the proposed AGLOH model is compared to other conventional models like GLCM-ISLSR, GLOH-ISLSR, AGLOH-ISLSR-LA, and AGLOH-ISLSR-WOA related to proposed ISLSR classification, which is illustrated in Fig. 4. The accuracy of AGLOH-ISLSR-LMWOA is very high for 40% learning, and it is 0.12%, 11.57% better than GLOH-ISLSR and GLCM-ISLSR, respectively. For 60% learning performance the proposed AGLOH-ISLSR is 39.06% and 18.16% better from GLOH-ISLSR and GLCM-ISLSR respectively. For 70% learning, the proposed AGLOH-ISLSR-LMWOA is 67.41% and 20.3% superior to GLOH-ISLSR and GLCM-ISLSR, respectively. The sensitivity of AGLOH-ISLSR-LMWOA is high, and for 40% learning, the developed model is 0.29% and 56.43% better than GLOH-ISLSR and GLCM-ISLSR, respectively. For 70% of learning, the developed model is 65.71% better than the GLOH-ISLSR model. The specificity of AGLOH-ISLSR-LMWOA is 0.20% and 66.53% superior to GLOH-ISLSR and GLCM-ISLSR, respectively.

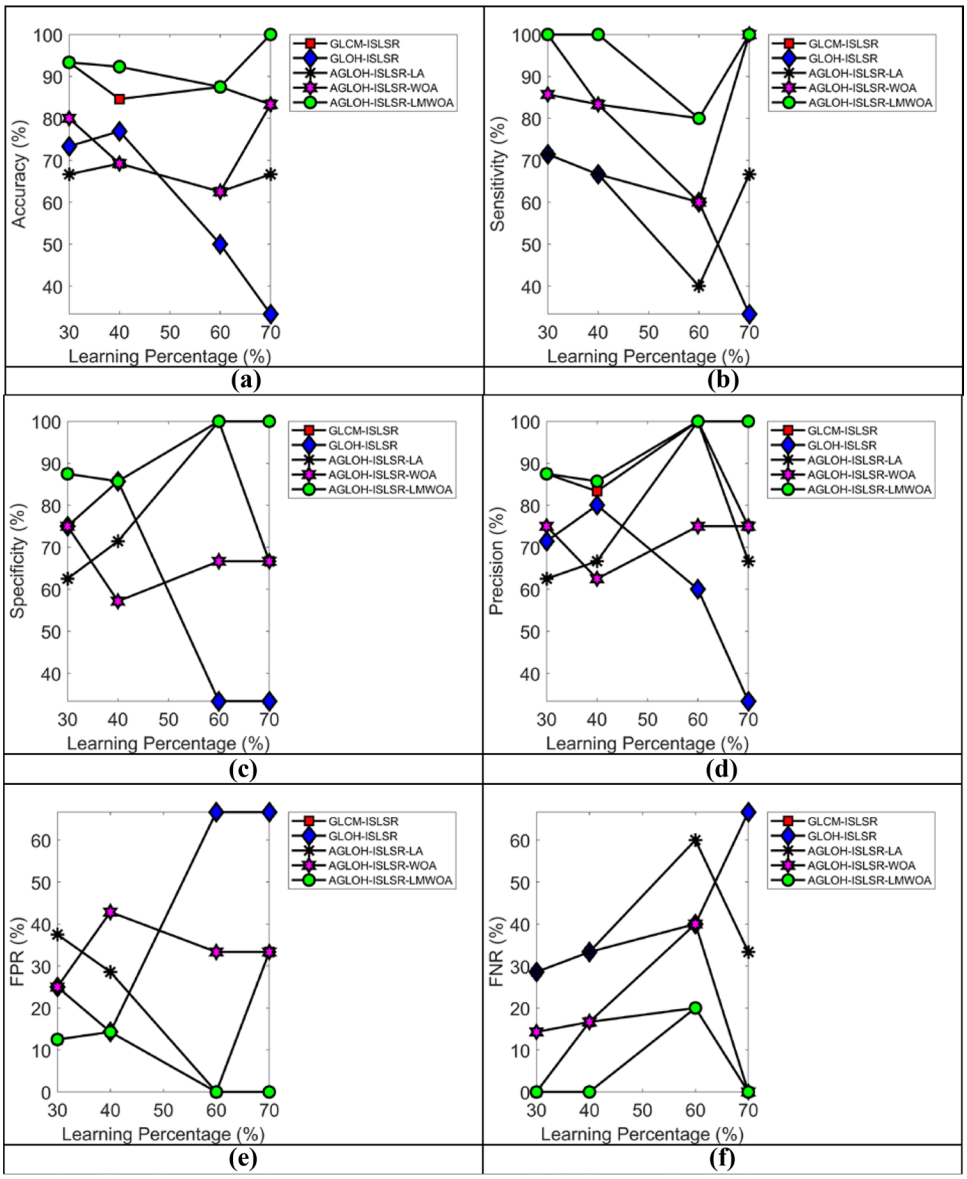

Fig. 4 Analysis on feature performances of proposed and existing feature extraction methods **a** Accuracy, **b** Sensitivity, **c** Specificity, **d** Precision, **e** FPR, **f** FNR, **g** NPV, **h** FDR, **i** F1-score, **j** MCC

Similarly, the analysis is made for negative measures. From the analysis, it is observed that the FPR of proposed AGLOH-ISLSR-LMWOA is very low, for 60% learning; the proposed AGLOH-ISLSR-LMWOA is 0.92% and 50.84% superior to GLOH-ISLSR and GLCM-ISLSR, respectively. The FNR of the proposed AGLOH-ISLSR-LMWOA is 3.52% and 52.31% better from the conventional GLOH-ISLSR and GLCM-ISLSR, respectively. The FDR of developed AGLOH-ISLSR-LMWOA is 33.08% and 37.88% better than GLOH-ISLSR and GLCM-ISLSR, respectively. The overall analysis shows the superiority of the proposed feature.

5.3 Classifier performance

The efficiency of the proposed AGLOH-ISLSR-LMWOA classifier is proved by comparing it with other existing classifiers like AGLOH-SVM, AGLOH-NN, AGLOH-LDCA, AGLOH-ISLSR-LA, and AGLOH-ISLSR-WOA, which is illustrated in Fig. 5. From the figure, it is observed that proposed AGLOH-ISLSR-LMWOA attained high accuracy for 40% learning, which is 11.95%, 75.1%, and 63.21% better than AGLOH-LDCA, AGLOH-NN, and AGLOH-SVM, respectively. For 60% of learning, the proposed AGLOH-ISLSR-LMWOA is 42.55% and 57.29% better

Fig. 4 (continued)

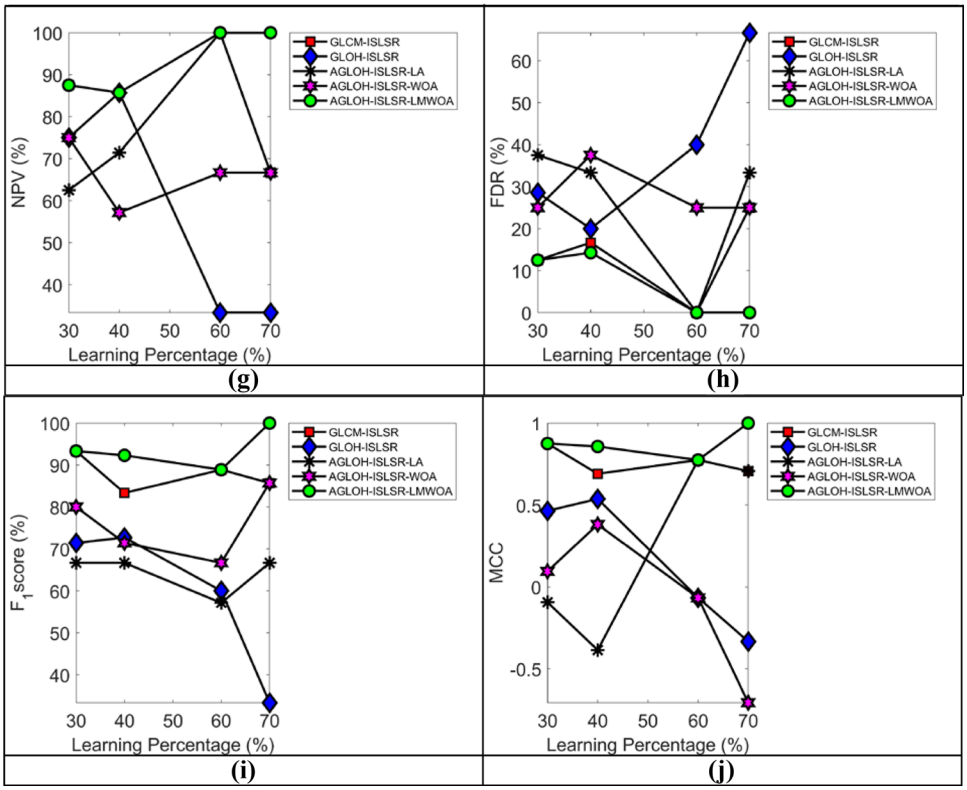

than AGLOH-NN, AGLOH-SVM, respectively. For 70% of learning, the proposed AGLOH-ISLSR-LMWOA is 68.90% superior to the AGLOH-NN method. The sensitivity of proposed AGLOH-ISLSR-LMWOA for 40% learning is 32.15% and 81.85% better than AGLOH-LDCA, AGLOH-NN, and AGLOH-SVM, respectively. For 70% learning, the developed AGLOH-ISLSR-LMWOA is 56.96% and 62.5% better from AGLOH-LDCA and AGLOH-NN, respectively. The specificity of proposed AGLOH-ISLSR-LMWOA for 40% learning is 52.20% and 34.80% better from AGLOH-NN and AGLOH-SVM respectively. For 60% of learning, the proposed AGLOH-ISLSR-LMWOA is better than the AGLOH-LDCA model. The precision of the proposed AGLOH-ISLSR-LMWOA is very high for 40% learning, which is 5.11% and 82.26% better than AGLOH-LDCA and AGLOH-SVM, respectively. For 60% of learning, the proposed AGLOH-ISLSR-LMWOA is 22.04% and 47.47% better from AGLOH-LDCA and AGLOH-NN, respectively. The NPV of proposed AGLOH-ISLSR-LMWOA for 40% learning is high, which is 50.52% and 34.11% better than AGLOH-NN and AGLOH-SVM, respectively.

From the negative measure analysis, it is evident that the FPR of proposed AGLOH-ISLSR-LMWOA for 40% learning is 75.77% and 66.58% superior to AGLOH-NN and AGLOH-SVM, respectively. The FNR of proposed AGLOH-ISLSR-LMWOA for 40% learning is 51.20% and 64.07% better than AGLOH-LDCA and AGLOH-SVM, respectively. Thus, the proposed AGLOH-ISLSR-LMWOA proved its superiority over other conventional models.

5.4 Comparative analysis

The inclusive performance of varied combinations of feature extraction and classification is illustrated in Fig. 6. The performance of proposed AGLOH-ISLSR-LMWOA is compared over other combinations like GLOH-LDCA, GLOH-NN, GLOH-SVM, GLCM-LDCA, GLCM-NN, GLCM-SVM, AGLOH-ISLSR-LA and AGLOH-ISLSR-WOA. From the accuracy analysis for 30% learning, it is observed that the proposed method attained high accuracy, which is 16.15%, 50.12%, 13.57%, 89.54%, and 39.28% better from the models like GLOH-LDCA, GLOH-NN, GLOH-SVM, GLCM-LDCA, GLCM-NN, and GLCM-SVM, respectively. for 40% learning, the proposed model is 4.11%, 83.54%, and 24.73% better than GLOH-LDCA, GLOH-NN, and GLCM-NN, respectively. For 60% of learning, the proposed model is 23.36%, 52.65%, and 26.26% better from GLOH-LDCA, GLOH-NN, and GLCM-NN, respectively. While analyzing the sensitivity measure, it is observed that for 30% of learning, the proposed model is 27.03%, 28.36%, 81.37%, and 65.69% better than the models like GLOH-LDCA, GLCM-LDCA, GLCM-NN, and GLCM-SVM, respectively. For 40% of

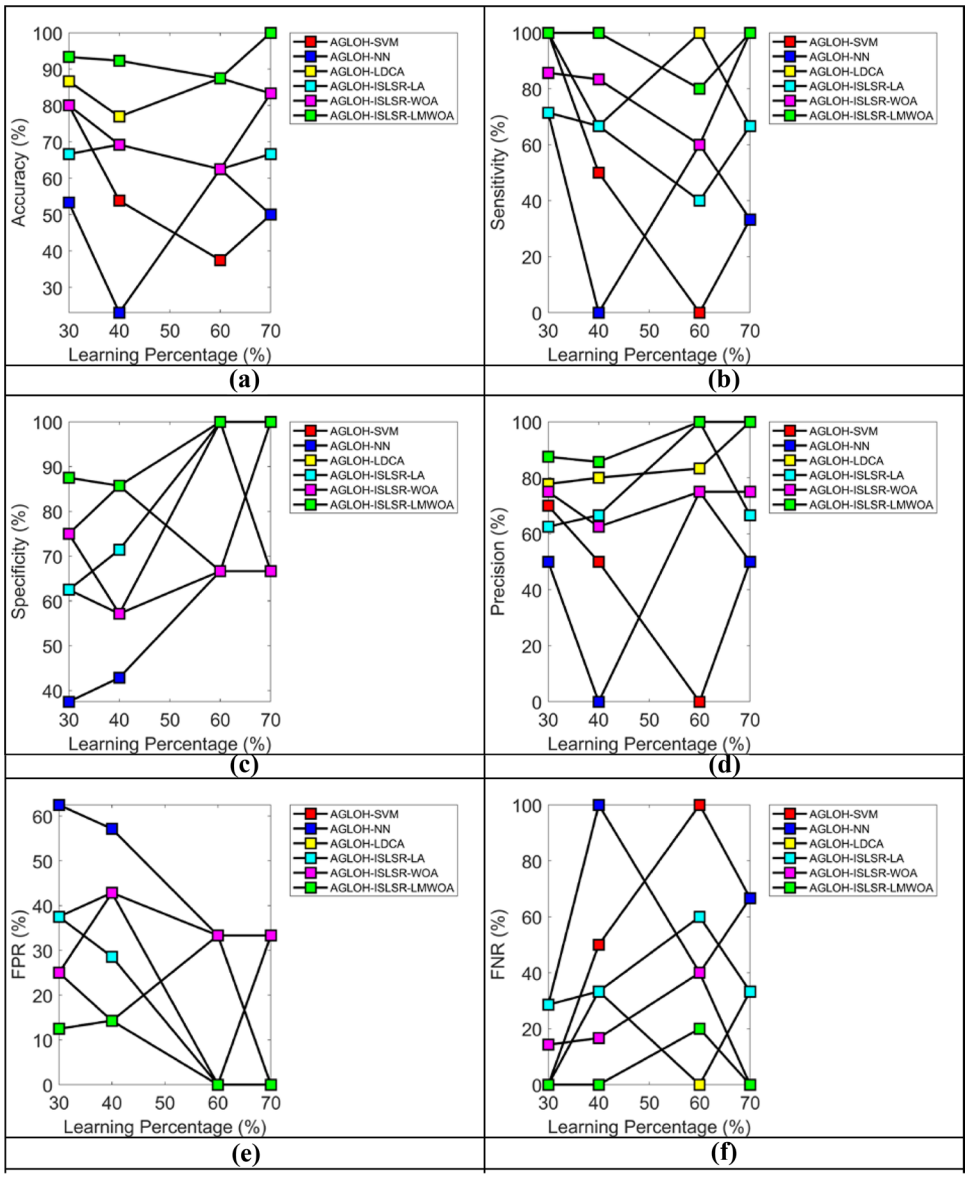

Fig. 5 Analysis on performances of proposed classifier and existing classifiers **a** Accuracy, **b** Sensitivity, **c** Specificity, **d** Precision, **e** FPR, **f** FNR, **g** NPV, **h** FDR, **i** F1-score, **j** MCC

learning, the proposed model is 27.42% and 54.09% better than GLOH-LDCA and GLCM-NN. For 60% learning, the proposed model is 35.69%, 74.01% and 49.20% superior to the methods like GLOH-LDCA, GLOH-NN, and GLCM-NN, respectively. for the precision measure, for 30% learning, the proposed AGLOH-ISLSR is 5.45%, 0.012%, 84.50% and 64.60% superior to GLOH-LDCA, GLOH-SVM, GLCM-NN, and GLCM-SVM, respectively. For 40% of learning, the proposed model is 2.55%, 93.54%, and 45.36% better from GLOH-LDCA, GLCM-NN, and GLCM-SVM, respectively. For 60% of learning, the developed model is 25.89%, 54.54%, and 95.69% better than GLOH-LDCA, GLOH-NN, and GLCM-NN, respectively. Thus, the analysis reviews the superiority of developed features for better diagnosing.

5.5 Performance efficiency

The overall performance of the proposed classifier is illustrated in Fig. 7. From the analysis of the negative measure, it is evident that FPR of proposed AGLOH-ISLSR-LMWOA is 6.25%, 74.13%, and 65.11% better than AGLOH-LDCA, AGLOH-NN, and AGLOH-SVM, respectively. FNR of proposed AGLOH-ISLSR is 52.63%, 81.63%, and 63.26% better from AGLOH-LDCA, AGLOH-NN, and AGLOH-SVM, respectively. FDR of proposed AGLOH-ISLSR is 5.26%, 81.63% and 63.26% superior to AGLOH-LDCA, AGLOH-NN, and AGLOH-SVM, respectively.

The accuracy of AGLOH-ISLSR is 15.49%, 63.41%, and 36.58% better than AGLOH-LDCA, AGLOH-NN, and AGLOH-SVM, respectively. The sensitivity of AGLOH-ISLSR-LMWOA is 30.64%, 87.65% and 39.50% superior

Fig. 5 (continued)

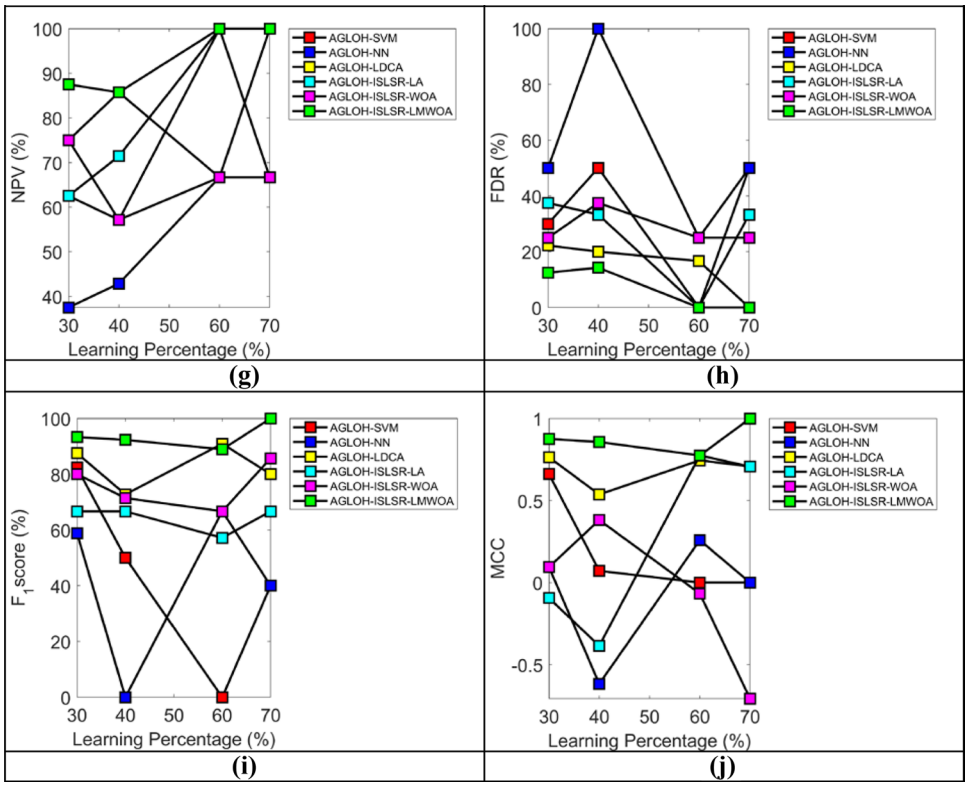

to AGLOH-LDCA, AGLOH-NN, and AGLOH-SVM, respectively. The specificity of the proposed AGLOH-ISLSR is 1.23%, 42.68%, and 36.58% better from AGLOH-LDCA, AGLOH-NN, and AGLOH-SVM, respectively. The precision of AGLOH-ISLSR is 3.89%, 85%, and 36.25% better from AGLOH-LDCA, AGLOH-NN, and AGLOH-SVM, respectively. NPV of AGLOH-ISLSR is 2.46%, 50.60%, and 36.14% better from AGLOH-LDCA, AGLOH-NN, and AGLOH-SVM respectively. The overall analysis shows the superiority of the proposed model.

The performance of the proposed feature is shown in Fig. 8. The FPR of proposed AGLOH-ISLSR-LMWOA is low, which is 5.55% and 82.65% better than GLOH-ISLSR and GLCM-ISLSR, respectively. FDR of proposed AGLOH-ISLSR-LMWOA is low, which is 5.26% and 68.96% superior to GLOH-ISLSR and GLCM-ISLSR, respectively. Further, the accuracy of the proposed AGLOH-ISLSR-LMWOA is high, which is 6.41% and 93.02% better from GLOH-ISLSR and GLCM-ISLSR, respectively. The specificity of AGLOH-ISLSR-LMWOA is 1.20% and 82.14% superior to GLOH-ISLSR and GLCM-ISLSR, respectively. The precision of AGLOH-ISLSR-LMWOA is 3.79% and 70.83% better from the models like GLOH-ISLSR and GLCM-ISLSR, respectively. The F_1 Score of AGLOH-ISLSR-LMWOA is 3.84% and 30.64% better than GLOH-ISLSR and GLCM-ISLSR, respectively. Hence, the overall analysis proved the proficiency of the proposed feature over conventional features.

The overall performance of the proposed model is compared to other combinations, which is illustrated in Fig. 9. It is observed that the accuracy of the proposed model is 9.09%, 86.66%, 6.32%, 18.30%, 16.66%, and 71.42% better than GLOH-LDCA, GLOH-NN, GLOH-SVM, GLCM-LDCA, GLCM-NN, and GLCM-SVM, respectively. The sensitivity of the proposed model is 12.5%, 88.37%, 17.39%, 59.25%, 56.79%, and 6.57% better from GLOH-LDCA, GLOH-NN, GLOH-SVM, GLCM-LDCA, GLCM-NN, and GLCM-SVM, respectively. moreover, the specificity of the proposed model is 1.20% better than GLOH-LDCA and GLOH-NN, and it is 2.43%, 9.09%, 7.69%, and 90.90% better than GLOH-SVM, GLCM-LDCA, GLCM-NN, and GLCM-SVM, respectively. F_1 Score of the proposed model is 7.89%, 95.23%, 6.49%, 54.71%, 51.85%, and 34.42% better than GLOH-LDCA, GLOH-NN, GLOH-SVM, GLCM-LDCA, GLCM-NN, and GLCM-SVM, respectively. the overall performance has proved that the proposed model outperforms other models in terms of efficient mass detection.

6 Conclusion

This paper has adopted an enhanced abdominal mass detection model using US images. It has achieved in two phases: feature extraction and classification. Texture features were extracted using the AGLOH model and the classification was carried out using the optimized ISLSR model, where the coefficient

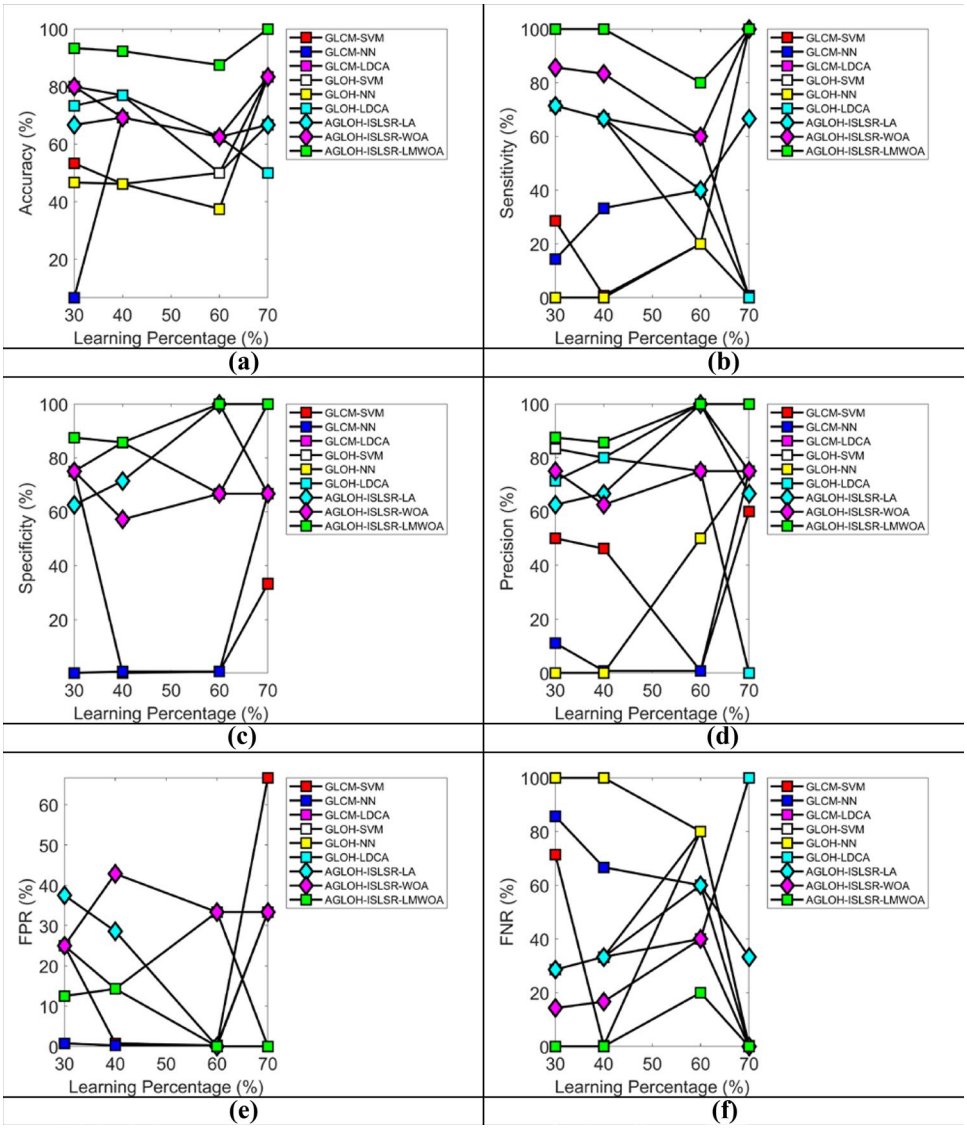

Fig. 6 Overall comparative analysis of proposed and conventional methods **a** Accuracy, **b** Sensitivity, **c** Specificity, **d** Precision, **e** FPR, **f** FNR, **g** NPV, **h** FDR, **i** F1-score, **j** MCC

matrix was optimally tuned using a new hybrid algorithm. The proposed model was compared with other conventional models. The accuracy of AGLOH-ISLSR-LMWOA is very high for 40% learning, and it is 0.12%, 11.57% better than GLOH-ISLSR and GLCM-ISLSR respectively. For 60% learning performance the proposed AGLOH-ISLSR-LMWOA is 39.06% and 18.16% better from GLOH-ISLSR and GLCM-ISLSR respectively. For 70% learning, the proposed AGLOH-ISLSR-LMWOA is 67.41% and 20.3% superior to GLOH-ISLSR and GLCM-ISLSR respectively. The sensitivity of AGLOH-ISLSR-LMWOA is high, and for 40% learning, the developed model is 0.29% and 56.43% better than GLOH-ISLSR and GLCM-ISLSR respectively. For 70% of learning, the developed model is 65.71% better than the GLOH-ISLSR model. The specificity of AGLOH-ISLSR is 0.20% and 66.53% superior to GLOH-ISLSR and GLCM-ISLSR respectively. Similarly, the analysis is made for negative measures. From the analysis, it is observed that the FPR of proposed AGLOH-ISLSR is very low, for 60% learning; the proposed AGLOH-ISLSR-LMWOA is 0.92% and 50.84% superior to GLOH-ISLSR and GLCM-ISLSR respectively. The FNR of the proposed AGLOH-ISLSR is 3.52% and 52.31% better from the conventional GLOH-ISLSR and GLCM-ISLSR respectively. The FDR of developed AGLOH-ISLSR-LMWOA is 33.08% and 37.88% better than GLOH-ISLSR and GLCM-ISLSR respectively. The overall analysis shows the efficacy of the proposed model by accurately detecting the abdominal mass in an image.

Fig. 6 (continued)

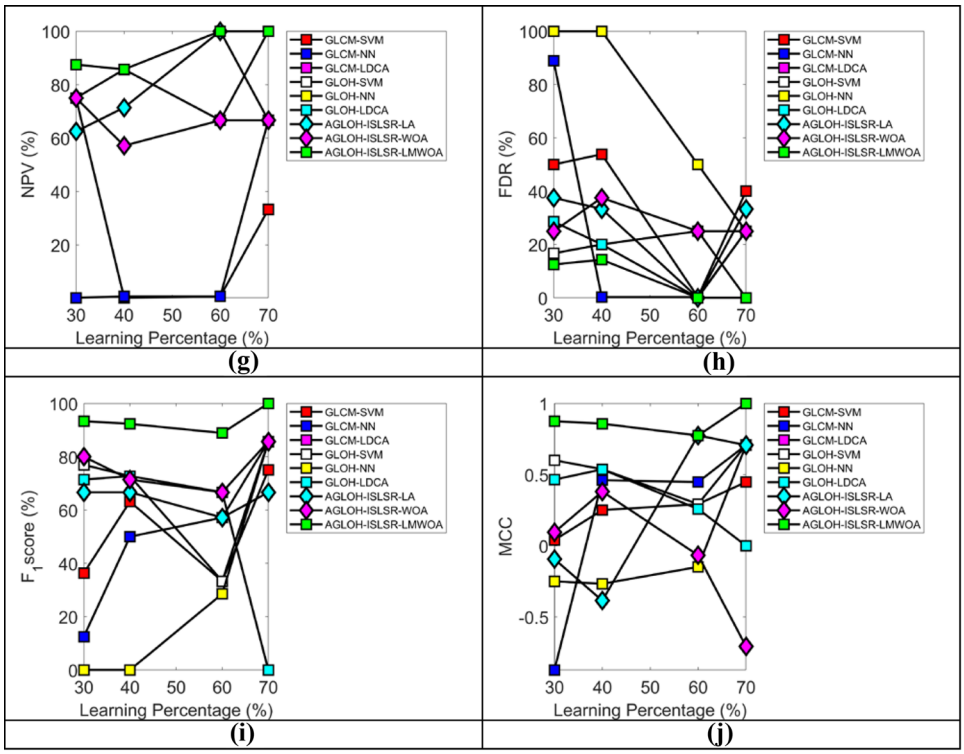

Fig. 7 Overall performance of proposed classifier **a** Positive measure, **b** negative measure

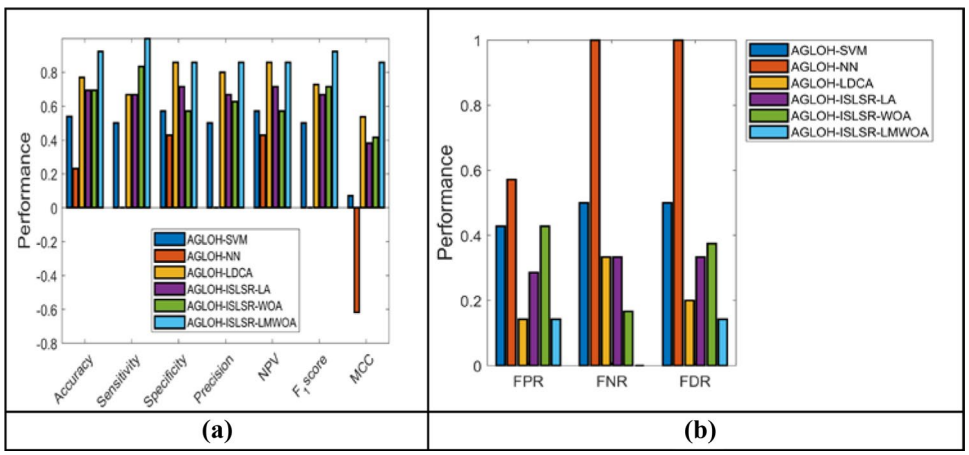

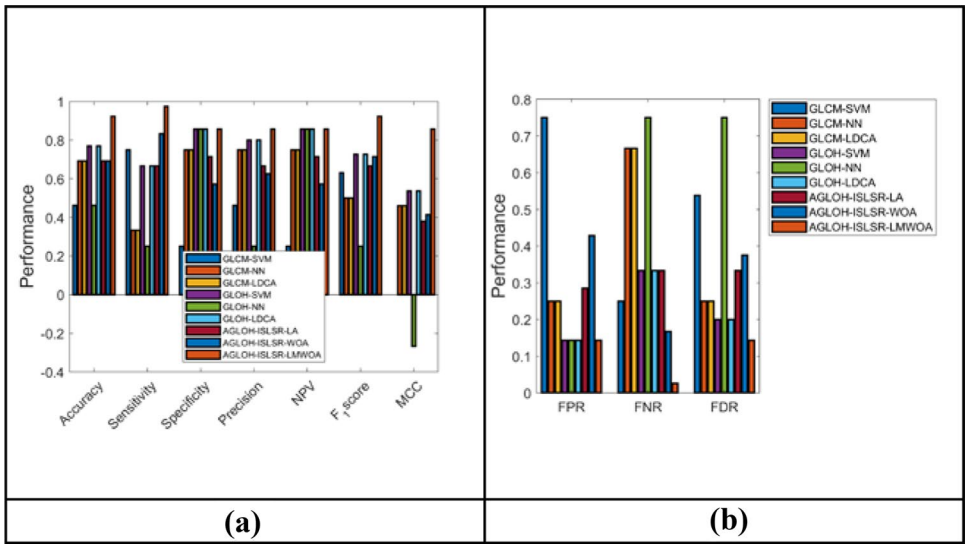

Fig. 8 Overall performance of the proposed feature **a** Positive measure, **b** negative measure

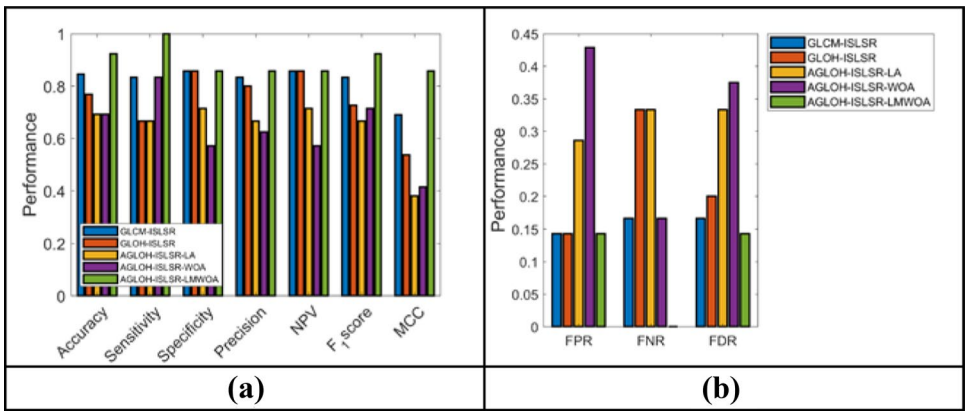

Fig. 9 Overall performance of proposed over other combinations

References

1. Wu F, Wang ZB, Zhu H, Chen WZ, Zou MDJZ, Bai MDJ, Li MDKQ, Jin MDCB, Xie MDFL, Su MDHB (2005) Feasibility of US-guided high-intensity focused ultrasound treatment in patients with advanced pancreatic cancer: initial experience. Radiology 236:1034–1040
2. Bhagat S, Gauba N, Singh S, Singh A, Mahal GBS (2006) Assessment and comparison of abdominal masses by sonography and computed tomography. J Evol Med Dental Sci 3(01):84–94
3. Mashayekhi R, Parekh VS, Faghih M, Singh VK, Zaheer A (2020) Radiomic features of the pancreas on CT imaging accurately differentiate functional abdominal pain, recurrent acute pancreatitis, and chronic pancreatitis. Eur J Radiol 123:108778
4. Cao CX, Sharib JM, Blanco AM, Goldberg D, Kirkwood KS (2020) Abdominal imaging of pancreatic cysts and cyst-associated pancreatic cancer in BRCA1/2 mutation carriers: a retrospective cross-sectional study. J Am Coll Surgeons 230(1):53–63
5. Disseldorp EMJ, Dronkelaar JJ, Pluim JPW, Vosse FN, Lopata RGP (2020) ultrasound based wall stress analysis of abdominal aortic aneurysms using multiperspective imaging. Eur J Vasc Endovasc Surg 59(1):81–91
6. Nasser MA, Melendez J, Moreno A, Omer OA, Puig D (2017) Breasttumor classification in ultrasound images using texture analysis and super-resolution methods. Eng Appl Artif Intell 59:84–92
7. Singh BK, Verma K, Thoke AS (2016) Fuzzy cluster based neural network classifier for classifying breast tumors in ultrasound images. Expert Syst Appl 66:114–123
8. Drukker K, Giger ML, Vyborny CJ, Mendelson EB (2004) Computerized detection and classification of cancer on breast ultrasound. Acad Radiol 11(5):526–535
9. Cheng HD, Shan J, Ju W, Guo Y, Zhang L (2010) Automated breast cancer detection and classification using ultrasound images: a survey. Pattern Recognit 43(1):299–317
10. Shen WC, Chang RF, Moon WK (2007) Computer aided classification system for breast ultrasound based on breast imaging reporting and data system (BI-RADS). Ultrasound Med Biol 33(11):1688–1698
11. Bhatnagar K, Gupta SC (2017) Investigating and modeling the effect of laser intensity and nonlinear regime of the fiber on the optical link. J Opt Commun 38(3):341–353
12. Yarrapragada KSSR, Krishna BB (2017) Impact of tamanu oil-diesel blend on combustion, performance and emissions of diesel engine and its prediction methodology. J Braz Soc Mech Sci Eng 39(5):1797–1811
13. Le Y, Xu X, Zha L, Zhao W, Zhu Y (2015) Tumor boundary detection in ultrasound imagery using multi-scale generalized gradient vector flow. J Med Ultrason 42(1):25–38

14. Lo C, Shen YW, Huang CS, Chang RF (2014) Computer-aided multiviewtumor detection for automated whole breast ultrasound. Ultrason Imaging 36(1):3–17
15. Burnside ES, Drukker K, Li H, Bonaccio E, Zuley M, Ganott M, Net JM, Sutton EJ, Brandt KR, Whitman GJ, Conzen SD, Lan L, Ji Y, Zhu Y, Jaffe CC, Huang EP, Freymann JB, Kirby JS, Morris EA, Giger M (2016) Using computer-extracted image phenotypes from tumors on breast magnetic resonance imaging to predict breast cancer pathologic stage. Cancer 122(5):748–757
16. Curiel L, Souchon R, Rouvière O, Gelet A, Chapelon JY (2005) Elastography for the follow-up of high-intensity focused ultrasound prostate cancer treatment: initial comparison with MRI. Ultrasound Med Biol 31(11):1461–1468
17. Hatimota P, Vashist S, Aggarwal K, Kapoor A, Gupta NP (2005) Spectrum of US and CT findings in renal neoplasms with pathologic correlation. Indian J Radiol Imaging 15(1):117–125
18. Qiu SQ, Zeng HC, Zhang F, Chen C, Huang WH, Pleijhuis RG, Wu JD, Dam GM, Zhang GJ (2016) A nomogram to predict the probability of axillary lymph node metastasis in early breast cancer patients with positive axillary ultrasound. Sci Rep 6:21196
19. Jesneck JL, Lo JY, Baker JA (2007) Breast mass lesions: computer-aided diagnosis models with mammographic and sonographic descriptors. Radiology 244(2):390–398
20. Crystal P, Strano SD, Shcharynski S, Koretz MJ (2003) Using sonography to screen women with mammographically dense breasts. AJR Am J Roentgenol 181(1):177–182
21. Kozegar E, Soryani M, Behnam H, Salamati M, Tan T (2017) Breast cancer detection in automated 3D breast ultrasound using iso-contours and cascaded RUSBoosts. Ultrasonics 79:68–80
22. Elyasi I, Pourmina MA, Moin MS (2016) Speckle reduction in breast cancer ultrasound images by using homogeneity modified Bayes shrink. Measurement 91:55–65
23. Shan J, Cheng HD, Wang Y (2012) Completely automated segmentation approach for breast ultrasound images using multiple-domain features. Ultrasound Med Biol 38(2):262–275
24. Wang B, Cao T, Dai Y, Liu DC (2010) Ultrasound speckle reduction via super resolution and nonlinear diffusion. In: Asian conference on computer vision, pp 130–139
25. Zhang F, Yoo YM, Koh LM, Kim Y (2007) Nonlinear diffusion in Laplacian pyramid domain for ultrasonic speckle reduction. IEEE Trans Med Imaging 26(2):200–211
26. Gu P, Lee WM, Roubidoux MA, Yuan J, Wang X, Carson PL (2016) Automated 3D ultrasound image segmentation to aid breast cancer image interpretation. Ultrasonics 65:51–58
27. Pons G, Martí R, Ganau S, Sentís M, Martí J (2014) Computerized detection of breast lesions using deformable part models in ultrasound images. Ultrasound Med Biol 40(9):2252–2264
28. Moon WK, Lee YW, Huang YS, Lee SH, Bae MS, Yi A, Huang CS, Chang RF (2017) Computer-aided prediction of axillary lymph node status in breast cancer using tumor surrounding tissue features in ultrasound images. Comput Methods Programs Biomed 146:143–150
29. Drukker K, Giger ML, Horsch K, Kupinski MA, Vyborny CJ, Mendelson EB (2002) Computerized lesion detection on breast ultrasound. Med Phys 29(7):1438–1446
30. Guo Y, Wang Y, Hou T (2011) Speckle filtering of ultrasonic images using a modified non local-based algorithm. Biomed Signal Process Control 6(2):129–138
31. Barbari M, Conti L, Rossi G, Simonini S (2017) Supply of wood as environmental enrichment material to post-weaning piglets. Agron Res 15(2):313–321
32. Oliveira KP, Ferreira CFS, Tinoco IFF, Andrade RR, Barbari M, Cruz VMF, Baptista FJF, Vieira MFA, Conti L, Rossi G (2018) Productive performance of broilers at the final stage of breeding submitted to different levels of metabolizable energy in different thermal environments. Eng Comput Agron Res 16(2):556–563
33. Morerira MG, Barbosa BDS, Ferraz GAS, Ferraz PFP, Rossi G, Iwasaki EM, Damasceno FA (2019) Design and construction of a low-cost remotely piloted aircraft for precision agriculture applications. Agron Res 17(5):1984–1992. https://doi.org/10.15159/AR.19.143
34. Jameel AS, Moshfeghyan M Factors affecting E-Commerce by E-learning. LAP Lambert Academic Publishing, Germany
35. Liang Y, Liu L, Xu Y, Xiang Y, Zou B (2011) Multi-task GLOH feature selection for human age estimation. In: 2011 18th IEEE international conference on image processing, Brussels, pp 565–568
36. Zheng W, Xin M, Wang X, Wang B (2014) A novel speech emotion recognition method via incomplete sparse least square regression. IEEE Signal Process Lett 21:5
37. Boothalingam R (2018) Optimization using lion algorithm: a biological inspiration from lion's social behavior. Evol Intel 11(1–2):31–52
38. Mirjalili S, Lewis A (2016) The whale optimization algorithm. Adv Eng Softw 95:51–67
39. Zhang Z, Salerno JJ, Yu PS (2003) Applying data mining in investigating money laundering crimes. In: Proceeding KDD '03 proceedings of the ninth ACM SIGKDD international conference on Knowledge discovery and data mining, pp 747–752
40. Meyer D, Leisch F, Hornik K (2003) The support vector machine under test. Neurocomputing 55(1–2):169–186
41. Guzmán F, Joty S, Màrquez L, Nakov P (2017) Machine translation evaluation with neural networks. Comput Speech Lang 45:180–200